ACS Sustainable Chemistry & Engineering

pubs.acs.org/journal/ascecg

Research Article

Inhibition Effect of Cooling Agent HFE-7100 on Lithium-Ion Batteries (LIBs) Thermal Runaway in the Immersion System

Biao Zhou,* Muying Ge, Kai Wang, Hideki Yoshioka, Jun Han, Linbo Qin, Zhenxiang Tao, Wei Wang, and Tao Chen

Cite This: https://doi.org/10.1021/acssuschemeng.5c00573

Read Online

ACCESS | Metrics & More | Article Recommendations

ABSTRACT: The methoxyperfluorobutane (HFE-7100) is a heat transfer fluid used widely in lithium-ion batteries (LIBs) thermal management. The thermal runaway of LIBs immersed in cooling liquid may yield a mixture of combustible gas inside the container. It threatens the safety of the immersion cooling system. In this work, the fundamental acknowledgment of the inhibition mechanism of HFE-7100 on LIBs thermal runaway management is investigated by the utilization of an Accelerating Rate Calorimeter (ARC) and a tube furnace test at an evaluated temperature. The characteristics of inhibition performance varying battery capacity are obtained. The pyrolysis products of HFE-7100 at an evaluated temperature and test conditions are obtained by Gas Chromatography (GC) and Gas Chromatography−Mass Spectrometry (GC-MS). Finally, the potential inhibition mechanism is proposed by the test results and previously available reaction pathways. It provides an insight for the understanding of the inhibition performance of heat transfer fluid used in an immersion cooling system.

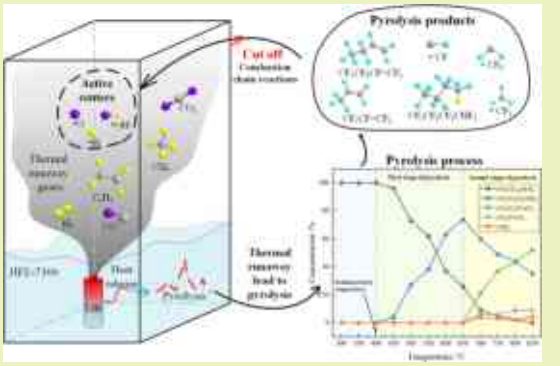

KEYWORDS: *lithium-ion batteries, heat transfer fluid, immersion cooling, the pyrolysis products, inhibition mechanism*

INTRODUCTION

Currently, the thermal runaway of LIBs has caused many fire cases, resulting in many serious disasters.[1] Immersion liquid cooling technology is widely used in LIBs systems due to its high heat transfer efficiency.[2] Immersion cooling liquids include fluorinated liquids, mineral oils, silicone oils, and water/glycol.[2] Most cooling liquids can effectively cover the operating temperature range of LIBs. However, mineral oils and silicone oils have flash points and may be ignited during thermal runaway, leading to severe consequences. Water/glycol-based coolants are electrically conductive, thus the encapsulation of LIBs is required for safe use as immersion coolants. In immersion cooling systems, the cooling liquid directly contacts LIBs, requiring fluids with low electrical conductivity. Fluorinated liquids are suitable solutions due to their dielectric properties and inertness.[3] Many hydrofluoroethers (HFEs) function as heat transfer fluids. Notably, HFE-7000, HFE-7100, HFE-7200, HFE-7300, and HFE-7500 show environmentally favorable properties, with GWP (global warming potential) values below 530 and ALT (atmospheric lifetime) under 5 years. Among them, HFE-7100 (methoxyperfluorobutane, C5H3OF9, CAS No. 163702-07-6) has excellent environmental properties, including an ODP (ozone depletion potential) of 0, a GWP of 320, and an ALT of 4.1 years.[4] Additionally, it is stable, nonflammable, and nonreactive, indicating good chemical compatibility.[5] Its low boiling point (61 °C at 1 atm) enables electronic components to operate at low working temperatures.[6] Therefore, it is widely used in immersion systems, such as energy storage systems (ESS) and data centers and so on.[7−11]

It is widely acknowledged that immersion liquid cooling systems primarily utilize the latent heat of the liquid coolant to absorb the heat generated by LIBs. However, even with immersion cooling, the thermal runaway behavior of LIBs still happens frequently,[12,13] releasing large quantities of combustible gases.[14,15] Regarding the immersion cooling system, the mixture of combustible gases generated from thermal runaway and the pyrolysis products of cooling agents would accumulate in the top part of the system, just as shown in Figure 1. The fire explosion risk of the gas mixture threatens the safety of the immersion system. This issue is critically important for the safety of immersion liquid cooling systems and warrants immediate attention and in-depth exploration. Therefore, it is crucial to investigate the impact of coolant pyrolysis products on the gas products generated during LIB thermal runaway.

Received: January 19, 2025
Revised: June 4, 2025
Accepted: June 5, 2025

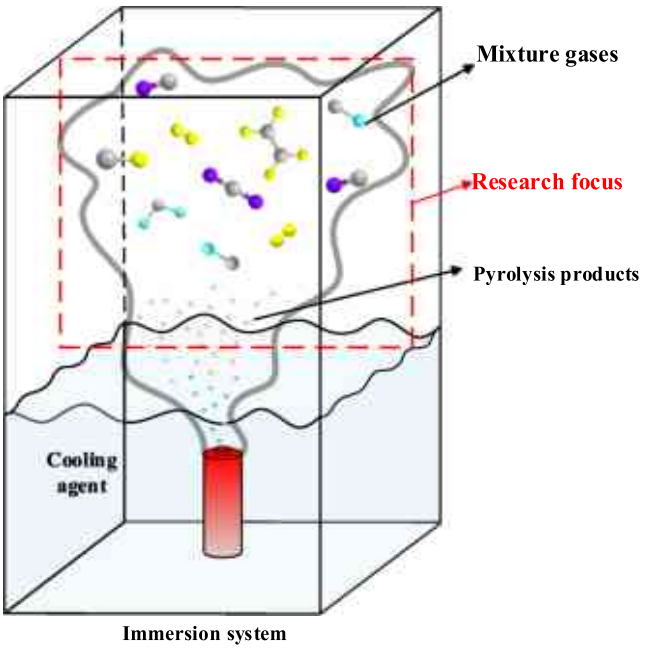

Figure 1. Gases distribution of the immersion system.

The immersion cooling system primarily has two effects: liquid cooling and the impact of pyrolysis products on thermal runaway and deflagration. On one hand, the liquid absorbs latent heat to achieve cooling. On the other hand, the impact of pyrolysis products from the cooling agent on the deflagration of LIBs. Currently, extensive research has been conducted on the effectiveness of liquid cooling.[16,17] Other works have been conducted on the characteristics of thermal runaway under immersion cooling conditions,[12] the composition of thermal runaway gases,[15] and the risks of these gases in confined spaces.[18] However, most current studies are concentrated on individual characteristics. There is a lack of research on the impact of pyrolysis products on thermal runaway and deflagration. In practice, gases from batteries and pyrolysis products of liquid coolants may accumulate in confined spaces under immersion cooling conditions. It needs to be taken into consideration. Some studies have discussed the pyrolysis components of fluorine-containing substances, such as $C_5F_{10}O$,[19] the $CH_2FOCHFO$ radical formed during the photolytic oxidation of HFE-152E,[20] as well as CF_3CF_3, $CF_3CF_2CF_3$, and $CF_3CF_2CF_2CF_3$.[21] Research on the pyrolysis components of HFE-7100 is currently lacking. Given the potential risks associated with immersion liquid cooling systems, it is essential to investigate the pyrolysis products that may arise when HFE-7100 is employed as a liquid coolant. In addition, although it has been confirmed that HFE-7100 pyrolysis products exert a certain inhibitory effect on the deflagration of LIB thermal runaway gases.[22] Until now, the specific inhibition mechanisms have not been realized. Therefore, research on the inhibition mechanisms of HFE-7100 pyrolysis products against

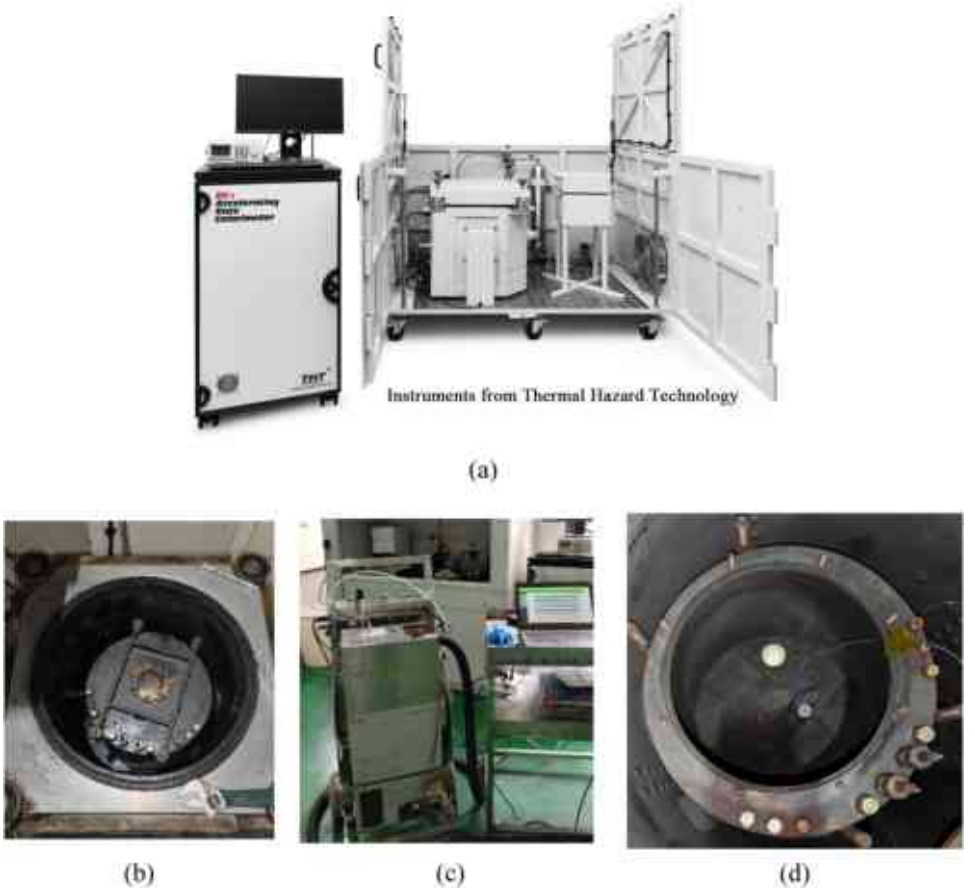

Figure 2. Description of ARC test and Fourier Transform Infrared Spectroscopy (a) ARC facility (b) the inner outlook of EV+ Calorimeter (c) Fourier Transform Infrared Spectroscopy (d) experimental setup.

https://doi.org/10.1021/acssuschemeng.5c00573
ACS Sustainable Chem. Eng. XXXX, XXX, XXX−XXX

the deflagration of LIB thermal runaway gases needs to be further explored.

In this work, the aim is to explore the inhibition mechanisms of HFE-7100 pyrolysis products against the deflagration of thermal runaway gases in confined space. To simplify the mechanism study, the heat absorption effect of the HFE-7100 immersion system is not considered, focusing only on the impact of HFE-7100 evaporation and pyrolysis products on thermal runaway and deflagration of LIBs. Experiments were conducted using an EV+ Accelerating Rate Calorimeter (ARC) on LIBs with capacities of 1800 mAh, 2000 mAh, 2500 mAh, and 2600 mAh, at 100% state of charge (SOC), with the addition of 2 g of HFE-7100. The inhibition effect of HFE-7100 on the deflagration of thermal runaway gas from LIBs of different capacities was investigated. Additionally, a self-designed pyrolysis kinetics testing platform was developed, incorporating gas chromatography (GC) and gas chromatography−mass spectrometry (GC-MS) for the qualitative and quantitative analysis of HFE-7100 pyrolysis gases. Finally, the inhibition mechanism of HFE-7100 pyrolysis products on the deflagration of thermal runaway gases under confined space conditions was revealed.

EXPERIMENTS AND METHODS

Materials. The 18650 is chosen as a typical cylindrical LIB. The cells are 18 mm in diameter and 65 mm in height, featuring nominal capacities of 1800, 2000, 2500, and 2600 mAh, a maximum charging voltage of 4.2 V, a cathode material of Li(NiMnCo)1/3O2, and an anode material of carbon. The LIB is supplied by Wuhan Zhongju Energy Technology Co., Ltd.. Before testing, the 18650 LIB was charged to 100% SOC, and then left to rest for 12 h to stabilize. HFE-7100 (99.7%) was purchased from 3 M China.

Accelerating Rate Calorimeter (ARC). The EV+ Accelerating Rate Calorimeter (ARC) instrument utilized in this research was produced by Thermal Hazard Technology,[23] as shown in Figure 2a. The EV+ is a cylindrical calorimeter with a diameter of 40 cm, a depth of 44 cm, 6 mm thick aluminum sides, and a lid and base made of 12 mm thick aluminum, as shown in Figure 2b. It is equipped with eight heaters and six thermocouples for measurement and control. Additionally, a Fourier transform infrared spectroscopy is connected externally to the ARC system to detect the composition of thermal runaway gases, as shown in Figure 2c.

The experiment focused on studying the impact of HFE-7100 on thermal runaway deflagration in LIBs with different capacities (1800, 2000, 2500, and 2600 mAh) at 100% SOC. Under immersion conditions, the intense heat release during the thermal runaway of LIBs can cause evaporation and pyrolysis of the cooling liquid. Clarifying the specific effects of HFE-7100 evaporation or pyrolysis products on thermal runaway is of significant importance. To simplify the mechanism study, only the impact of HFE-7100 pyrolysis products on deflagration within the immersion liquid cooling system was considered, while the heat absorption effect of the liquid was excluded. Thus, 2 g of HFE-7100 was used in the experiment to simulate the enrichment of mixed gases in the immersion cooling system during the evaporation and pyrolysis of the cooling liquid under immersion conditions.

Thus, the LIB thermal runaway experiments were divided into a control group and an HFE-7100-treated group. This study adopts the heat-wait-seek mode of ARC to systematically investigate thermal behavior, in order to emulate realistic temperature escalation scenarios encountered in practical battery operation. The battery samples were securely fastened to the bracket and subsequently placed within the ARC-sealed container. A high-precision balance was used to measure the 2 g of HFE-7100. It was placed in a crucible and loaded into a sealed ARC container near the battery sample, as shown in Figure 2d. Thermocouples, pressure sensors, and a Fourier transform infrared spectroscopy probe were installed and securely fixed. The container was promptly sealed, and the sealing performance and safety of the container were examined. The experiments were conducted under room temperature conditions (25 °C). The heat-wait-seek mode was employed, with the target set to 200 °C and a heating rate of 0.5 °C/min, to conduct precise thermal runaway experiments. Battery exothermic reactions were simulated and actual operating conditions were replicated during the experimental process. Data recording devices were used to monitor and record changes in temperature, pressure, and peak temperature ratio inside the container. Data below 45 °C were excluded from the analysis to better observe the characteristic parameters of lithium-ion battery thermal runaway.

Pyrolysis Kinetic Apparatus. A pyrolysis kinetic testing platform was independently designed in this study to conduct high-temperature pyrolysis experiments on HFE-7100. The experimental platform is primarily composed of a reactant injection system, a high-temperature-resistant reaction tube, a heating and temperature control system, as well as a drying, deacidification, and exhaust gas treatment system. The experimental platform is illustrated in Figure 3.

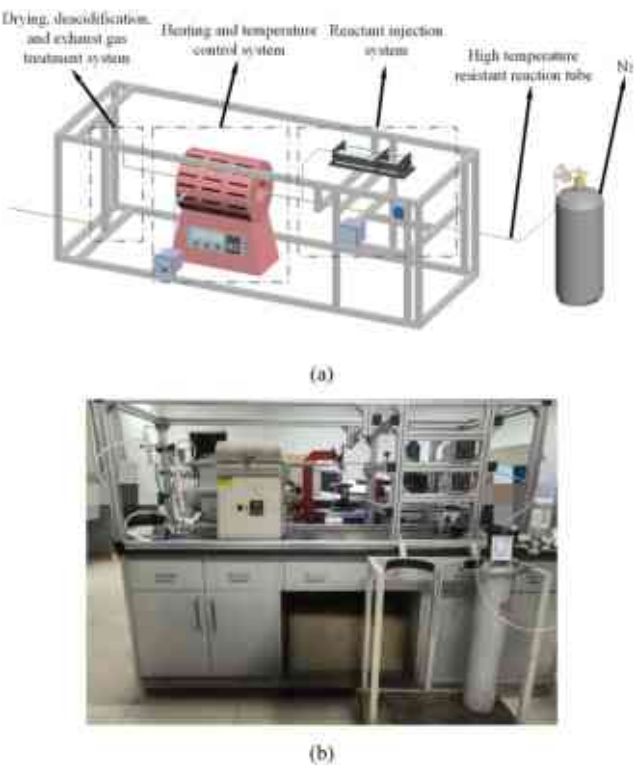

Figure 3. Testing platform of pyrolysis (a) schematic[24] (b) testing platform.

During the experiment, the tube furnace was slowly heated to the target experimental temperature (ranging from 300 to 850 °C). Nitrogen gas was continuously introduced during the heating process to remove reactive gases such as oxygen. The syringe pump was initiated once the tube furnace attained the target temperature, and a mixture of HFE-7100 and nitrogen gas was introduced at a constant flow rate. After residing in the constant temperature zone for a certain period, the gas passed through the acid removal device. A gastight manual syringe was used to collect the reaction gases between the drying, deacidification, and the exhaust gas treatment device to ensure the purity of the gas sample. The collected gases were then analyzed using GC-MS. Subsequently, the syringe pump was turned off, and the nitrogen flow rate was increased to remove residual gases from the tube furnace and experimental pipeline for exhaust gas treatment.

GC analysis was conducted using a Shimadzu GC-2014C gas chromatograph from Japan. The pyrolysis gases were analyzed online using a flame ionization detector (FID), with a DB-5MS column (30 m in length). Nitrogen was used as the carrier gas, with the column oven

https://doi.org/10.1021/acssuschemeng.5c00573
ACS Sustainable Chem. Eng. XXXX, XXX, XXX−XXX

Figure 4. Description of LIB samples (a) prior to test (b) after test.

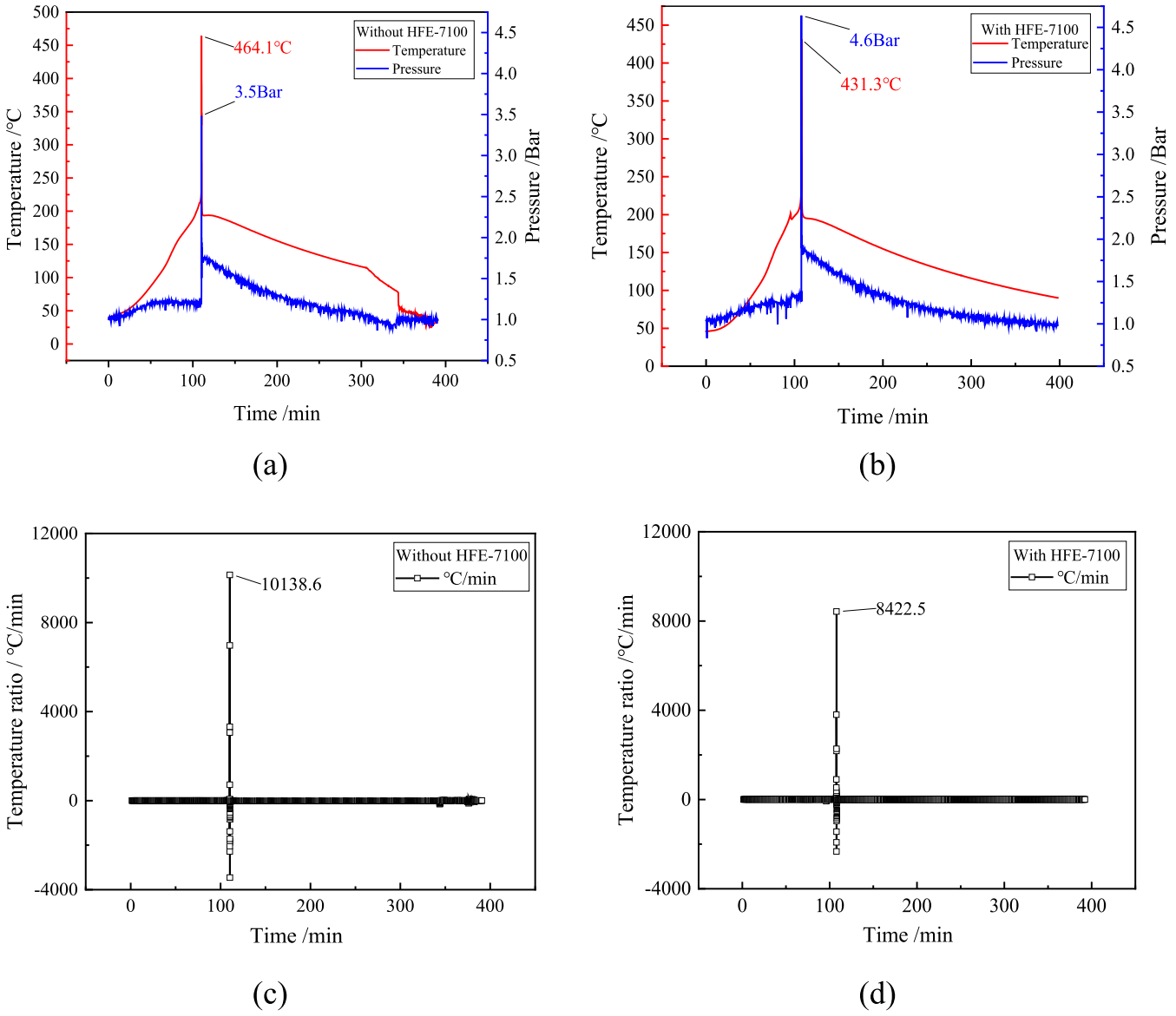

Figure 5. Temperature and pressure test results of thermal runaway (a) temperature and pressure distribution without HFE-7100 (b) with the addition of HFE-7100 (c) temperature ratio without HFE-7100 (d) with the addition of HFE-7100.

temperature set at 40 °C, the injection port temperature at 140 °C, and the detector temperature at 220 °C. The split ratio was set to 10:1. GC-MS analysis was performed using an Agilent 7890A-5975C GC-MS system from the United States, equipped with an HP-1MS column (30 m in length). Nitrogen was used as the carrier gas, with the vaporization chamber temperature set at 220 °C, and the transfer line temperature at 220 °C. The electron ionization (EI) source temperature of the mass spectrometer was set at 230 °C, with a split ratio of 10:1.

RESULTS AND DISCUSSION

Deflagration Inhibition Performance of HFE-7100 Based on ARC. To understand the inhibition effect of HFE-

https://doi.org/10.1021/acssuschemeng.5c00573
ACS Sustainable Chem. Eng. XXXX, XXX, XXX−XXX

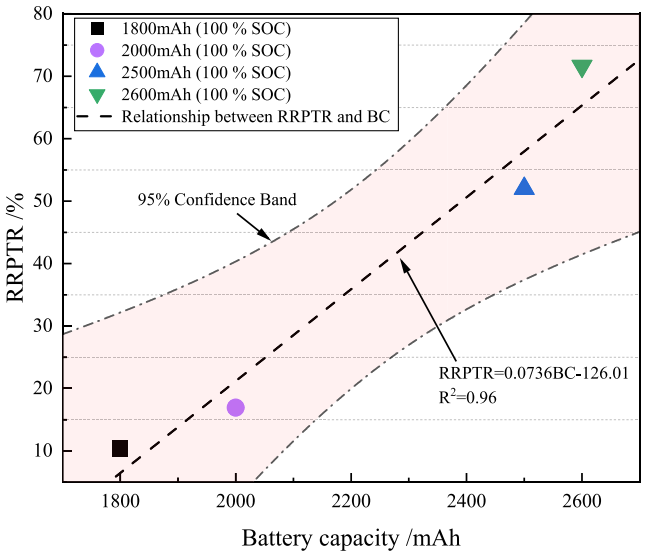

Figure 6. Relationship fitting line between RRPTR and BC.

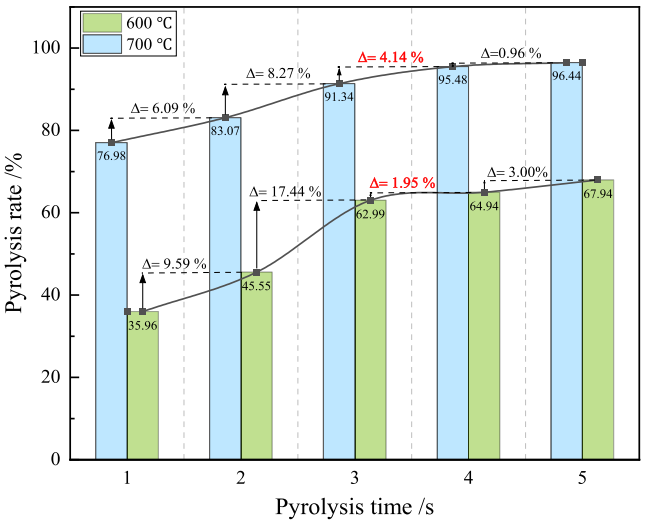

Figure 7. Relationship between the pyrolysis rate and pyrolysis time.

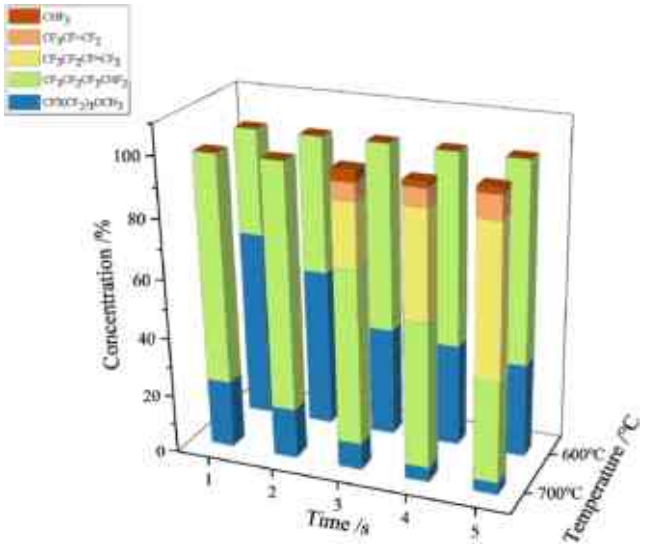

Figure 8. Relationship of pyrolysis product with time and temperature.

7100 on the deflagration of LIBs with different capacities, the temperature and pressure curves during the thermal runaway of LIBs were measured experimentally. The descriptions of LIB before and after the experiment are shown in Figure 4a,b.

Experimental results show that for 2000 mAh LIB, the peak thermal runaway temperature decreased from 464.1 to 431.3 °C and the peak pressure increased from 3.5 to 4.6 bar after adding HFE-7100 into the chamber. The peak temperature ratio decreased from 10138.6 °C/min to 8422.5 °C/min, which decreased by 16.9%, as shown in Figure 5.

In addition, the peak temperature ratio of the 1800 mAh LIB changed from 5447.3 °C/min to 4881.1 °C/min after adding HFE-7100, which decreased by 10.4%. The peak temperature ratio of thermal runaway of 2500 mAh and 2600 mAh LIBs were reduced by 51.9% and 71.6%, respectively, after the addition of HFE-7100.

The results demonstrate that the incorporation of HFE-7100 significantly lowers the peak temperature ratio during thermal runaway in LIB and effectively suppresses the deflagration of 18650 LIB. This is consistent with previous research.[22] The relationship between the reduction ratio of the peak temperature ratio (RRPTR) and battery capacity (BC) was fitted as $y = 0.0736x - 126.01$, with $R^2 = 0.96$. It was found that within a certain range, the inhibition effect is positively correlated with battery capacity, as shown in Figure 6. It is shown that within a certain range of battery capacity, HFE-7100 demonstrates greater efficacy in inhibiting thermal runaway deflagration in LIBs with larger capacities.

Pyrolysis Products of HFE-7100 Based on Tubular Pyrolysis Furnace. *Analysis of Pyrolysis Products.* The pyrolysis gas products at pyrolysis temperatures of 600, 700, and 750 °C with a pyrolysis time of 3 s were analyzed using GC-MS, and the results are shown in Table 1. According to Gas chromatograms and mass spectrometry data, after comparing and analyzing the molecular ion fragments against the standard chromatogram, it can be determined that in addition to the reactants, the main gas products produced by pyrolysis are 1H-PerfluoroButane ($CF_3CF_2CF_2CHF_2$), octafluoro-1-butene ($CF_3CF_2CF = CF_2$), hexafluoropropylene ($CF_3CF = CF_2$) and fluoroform (CHF_3).

Effect of Time and Temperature on the HFE-7100 Pyrolysis. The effect of pyrolysis temperature and time on pyrolysis rate and products was revealed by tests. The pyrolysis

Table 1. GC-MS Analysis of Gas Products from HFE-7100 at High Temperature

no.	mass-to-charge ratio (m/z)	substance
1	CH_3O^+(31); CF_2^+(50); CF_3^+(69); $C_2F_4^+$(100); $C_2F_5^+$(119);$C_3F_6^+$(150); $C_3F_7^+$(169);$C_4F_9^+$(219); $C_4F_9O^+$(235)	HFE-7100
2	CF^+(31); CF_2^+(50); CHF_2^+(51); CF_3^+(69); $C_2F_4^+$(100); $C_2F_5^+$(119); $C_3F_5^+$(131); $C_3F_6^+$(150); $C_3F_7^+$(169); $C_4F_7^+$(181); $C_4F_9^+$(219)	1H-perfluorobutane
3	CF^+(31); CF_2^+(50); CF_3^+(69); $C_2F_3^+$(81); $C_3F_3^+$(93); $C_2F_5^+$(119); $C_3F_5^+$(131); $C_3F_6^+$(150); C_4F6^+(162); $C_4F_7^+$(181); $C_5F_7^+$(200)	octafluoro-1-butene
4	CF^+(31); C_2F^+(43); CF_2^+(50); CF_3^+(69); $C_2F_3^+$(81); $C_3F_3^+$(93); $C_2F_4^+$(100); $C_3F_4^+$(112); $C_3F_5^+$(131)	hexafluoropropylene
5	CF^+(31); CHF_2^+(51); CF_3^+(69)	fluoroform

https://doi.org/10.1021/acssuschemeng.5c00573
ACS Sustainable Chem. Eng. XXXX, XXX, XXX−XXX

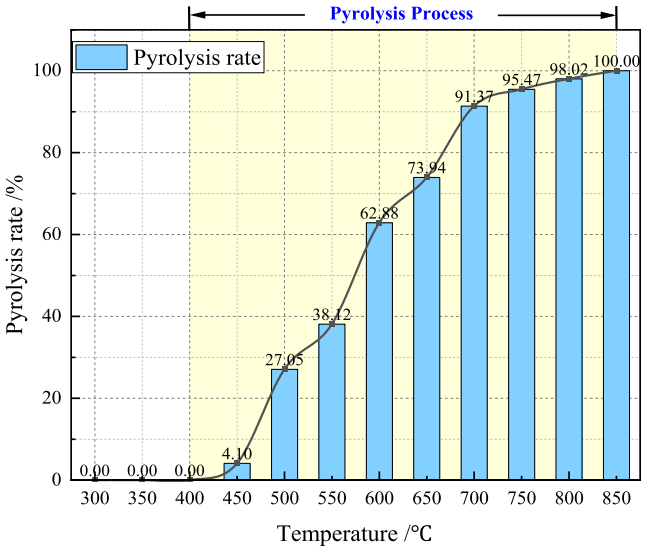

Figure 9. Relationship of pyrolysis rate with pyrolysis temperature.

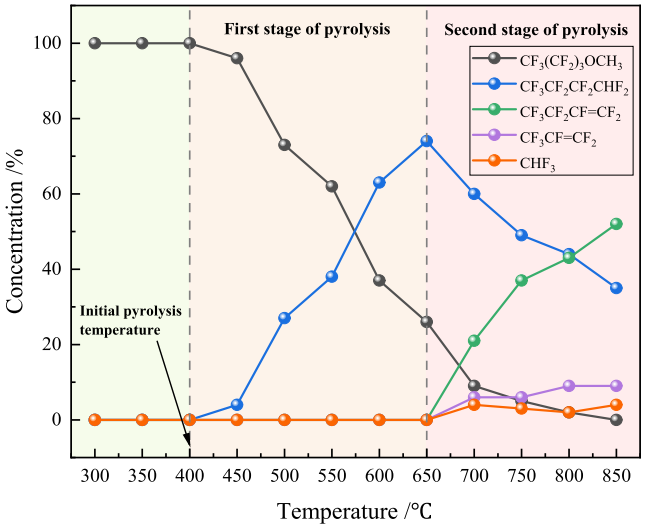

Figure 10. Relationship of pyrolysis product concentration and temperature.

Table 2. Reactions for Promoting the Deflagration and Main Reaction Pathways

no.	reactions
1	$CH_4 + O \rightarrow OH + CH_3$
2	$CH_3 + O_2 \rightarrow OH + CH_2O$
3	$CH_3 + O_2 \rightarrow O + CH_3O$
4	$H + CH_2O(+M) \rightarrow CH_3O(+M)$
5	$CH_2O + OH \rightarrow HCO + H_2O$
6	$OH + HCO \rightarrow H_2O + CO$
7	$H + HCO \rightarrow H_2 + CO$
8	$O + H_2 \rightarrow H + OH$
9	$H + O_2 \rightarrow O + OH$

gas products and pyrolysis rate at temperatures of 600 °C, and 700 °C, with a pyrolysis time of 1−5 s were analyzed.

Figure 7 shows that the pyrolysis rate increases with prolonged pyrolysis time at both 600 and 700 °C. At 600 °C,

Table 3. Reactions for Promoting the Deflagration

no.	reactions
1	$H + O_2 \rightarrow O + OH$
2	$OH + CO \rightarrow H + CO_2$
3	$H + HO_2 \rightarrow OH + OH$
4	$C_2H_3 + O_2 \rightarrow O + CH_2CHO$
5	$HO_2 + CH_3 \rightarrow OH + CH_3O$
6	$HCO(+M) \rightarrow H + CO(+M)$
7	$OH + C_2H_4 \rightarrow C_2H_3 + H_2O$

Table 4. Fire-Extinguishing Mechanism of Fluorine-Containing Groups

no.	reactions
1	$CHF_3 + H \rightarrow CF_3 + H_2$
2	$CHF_3 + OH \rightarrow CF_3 + H_2O$
3	$CHF_3 + O \rightarrow CF_3 + OH$
4	$CF_2O + H \rightarrow CFO + HF$
5	$CFO + OH \rightarrow CO_2 + HF$
6	$CFO + O \rightarrow CO_2 + F$
7	$CF + H_2O \rightarrow CHFO + H$
8	$CHFO + H \rightarrow CFO + H_2$
9	$CHFO + O \rightarrow CFO + OH$
10	$CHFO + M \rightarrow CO + HF$
11	$CO + O \rightarrow CO_2$
12	$CF + O_2 \rightarrow CFO + O$
13	$CF_2 + H \rightarrow CF + HF$
14	$CF_3O + M \rightarrow CF_2O + F$
15	$CF_3 + O_2 \rightarrow CF_3O + O$
16	$CF_3 + OH \rightarrow CF_2O + HF$
17	$CF_3 + H \rightarrow CF_2 + HF$
18	$CF_3 + O \rightarrow CF_2O + F$
19	$CF_2 + O \rightarrow CFO + F$
20	$CF_2 + O_2 \rightarrow CF_2O + O$
21	$CHF_2 + H \rightarrow CHF + HF$
22	$CHF + H \rightarrow CH + HF$
23	$CF + O \rightarrow CO + F$
24	$CF + OH \rightarrow CO + HF$
25	$CF_2 + OH \rightarrow CFO + HF$
26	$CF_2 + OH \rightarrow CF_2O + H$

the pyrolysis rate increases significantly during 1−3 s, with the pyrolysis rate increments per second at 2 and 3 s being 9.59 and 17.44%, respectively. At 3 s, the pyrolysis rate reaches 62.99%, and with further extension of the pyrolysis time, the increase in pyrolysis rate becomes relatively small. At 4 s, the pyrolysis rate increases by 1.95% compared to 3 s, and the increment per second at 5 s is 3.00%. At 700 °C, the pyrolysis rate increases from 76.98 to 91.34% when the pyrolysis time rises from 1 to 3 s. The increments in pyrolysis rate per second during 2−5 s are 6.09, 8.27, 4.14, and 0.96%, respectively. The point where pyrolysis is considered nearly complete is chosen when the increase in the pyrolysis rate per second is less than 5%.

https://doi.org/10.1021/acssuschemeng.5c00573
ACS Sustainable Chem. Eng. XXXX, XXX, XXX−XXX

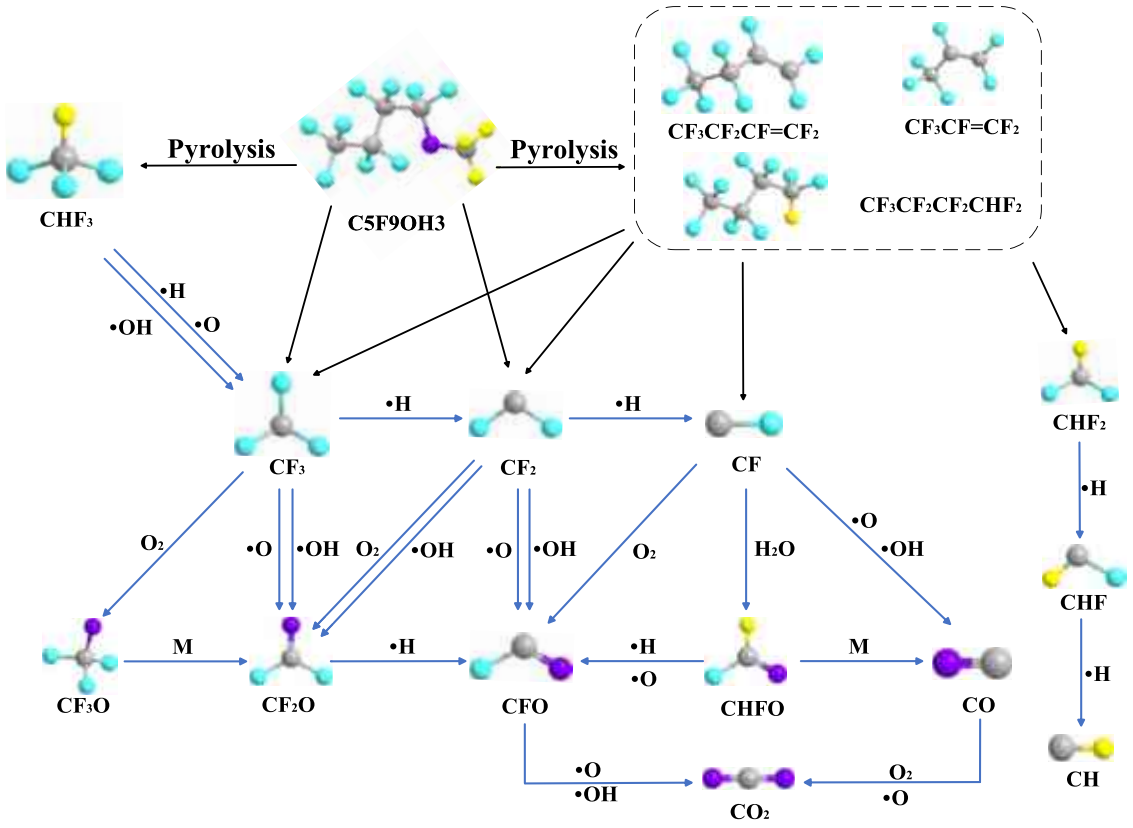

Figure 11. Reactions between fluorine-containing groups of HFE-7100 pyrolysis and free radicals.

Therefore, it can be drawn that the pyrolysis reaction is nearly completed when the pyrolysis time is 3 s. And it is obvious that the pyrolysis rate at 700 °C is higher than 600 °C.

Figure 8 shows the concentration of pyrolysis products of HFE-7100 at 600 °C, 700 °C, with a pyrolysis time of 1−5 s. It can be inferred from the figure that only one pyrolysis product $CF_3CF_2CF_2CHF_2$ was generated at 600 °C. At 700 °C, only $CF_3CF_2CF_2CHF_2$ is formed when the residence time is 1 or 2 s. In addition, when the residence time exceeds 3 s, four pyrolysis products are generated. The other three are $CF_3CF_2CF = CF_2$, $CF_3CF = CF_2$, and CHF_3. Additionally, at 700 °C, the composition of the pyrolysis products remains consistent when the residence time exceeds 3 s. And it does not change with an increase in pyrolysis time. However, the composition of pyrolysis products is influenced by temperature under the same pyrolysis duration, provided that pyrolysis progresses beyond a certain threshold. Therefore, it can be concluded that the pyrolysis time affects the pyrolysis rate, while the temperature determines the composition of the pyrolysis products once the pyrolysis reaches a certain point.

In conclusion, the composition of pyrolysis products of HEF-7100 is mainly related to the pyrolysis temperature. The extent of pyrolysis increases with higher temperatures, leading to more thorough decomposition. Beyond a certain threshold, the composition of HFE-7100 pyrolysis products becomes independent of pyrolysis time. According to Figure 7, it can be observed that when the pyrolysis time is 3 s, the pyrolysis is nearly complete. Therefore, in the subsequent content, the influence of different temperatures on the pyrolysis rate and pyrolysis product composition under the pyrolysis time of 3 s has been investigated.

Effect of Temperature on the Pyrolysis Rate of HFE-7100. The pyrolysis rate and initial decomposition temperature of HFE-7100 were determined by studying its pyrolysis process at temperatures ranging from 300 to 850 °C with pyrolysis times of 3 s.

Figure 9 shows that at a pyrolysis time of 3 s, the pyrolysis of HFE-7100 initiates at a temperature range of 400−450 °C. The pyrolysis rate rises rapidly with the increase in temperature when the temperature is within the range of 400−700 °C. And it reaches 91.37% at 700 °C. As the temperature further increases, the pyrolysis rate experiences a slight rise, eventually reaching 100% at 850 °C. Consequently, it can be concluded that the initial pyrolysis temperature of HFE-7100 is 400 °C. With the rise in temperature, the pyrolysis rate gradually increases until HFE-7100 is almost completely decomposed at 850 °C.

Effect of Temperature on the Pyrolysis Products of HFE-7100. Experiments were conducted to investigate the influence of pyrolysis temperature on the composition of HFE-7100 pyrolysis products. The analysis results from GC and GC-MS revealed the variation of pyrolysis products with temperatures between 300 and 850 °C.

Figure 10 shows the influence of different temperatures on the components of pyrolysis products at pyrolysis times of 3 s. The pyrolysis of HFE-7100 begins at 400 °C, producing $CF_3CF_2CF_2CHF_2$. Its concentration continues to rise with increasing temperature, reaching a peak of 74.21% at 650 °C, and then rapidly decreases to 35.45% at 850 °C. When the temperature exceeds 650 °C, products $CF_3CF_2CF = CF_2$ and small amounts of $CF_3CF = CF_2$ and CHF_3 begin to form. As the temperature rises, the concentration of $CF_3CF_2CF = CF_2$ increases rapidly, reaching 52.19% at 850 °C, while the concentrations of $CF_3CF = CF_2$ and CHF_3 are 9.04 and

https://doi.org/10.1021/acssuschemeng.5c00573
ACS Sustainable Chem. Eng. XXXX, XXX, XXX−XXX

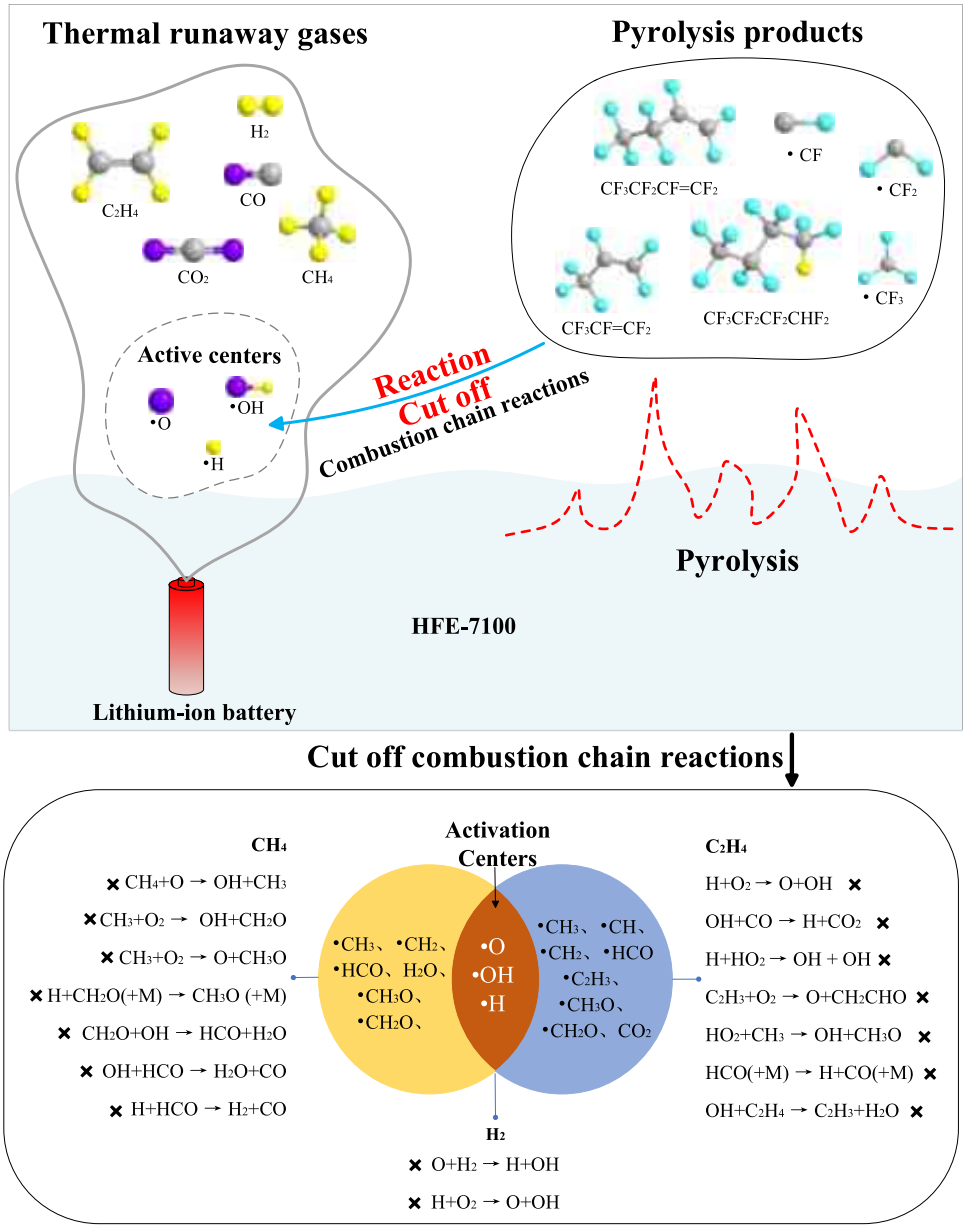

Figure 12. Mechanism of deflagration inhibition of HEF-7100.

4.15%, respectively. Throughout the pyrolysis process, the concentration of HFE-7100 continuously decreases, and it completely decomposed at 850 °C. In conclusion, the concentration of pyrolysis products rises as the temperature increases, initially dominated by $CF_3CF_2CF_2CHF_2$. As the temperature continues to rise, the concentration of $CF_3CF_2CF_2CHF_2$ starts to decrease, while three other products such as $CF_3CF_2CF = CF_2$, $CF_3CF = CF_2$, and small amounts of CHF_3 begin to form.

A comprehensive analysis of the above experimental results indicates that HFE-7100 begins to decompose at 400 °C and is nearly completely decomposed by 850 °C. According to the analysis results of pyrolysis gas products from GC and GC-MS, the gaseous products generated during the pyrolysis process mainly include $CF_3CF_2CF_2CHF_2$, $CF_3CF_2CF = CF_2$, $CF_3CF = CF_2$, CHF_3.

Proposal of Potential Inhibition Mechanism. Analysis of Fourier-transform infrared spectroscopy measurements reveals that multiple gases are generated during the thermal runaway of LIBs, primarily including H_2, CH_4, C_2H_4, HF, HCl, CO, and CO_2. Most of these are combustible gases, primarily due to intense redox reactions occurring during the thermal runaway of LIBs.[15,25−27]

In addition, the peak temperature during thermal runaway can reach approximately 400−800 °C, at which point the pyrolysis of HFE-7100 may produce compounds such as $CF_3CF_2CF_2CHF_2$, $CF_3CF_2CF = CF_2$, $CF_3CF = CF_2$, and CHF_3.

To elucidate the inhibition mechanism of HFE-7100 on the deflagration of LIBs, this study focuses on the reactions between the pyrolysis products of HFE-7100 and the combustible gases generated during thermal runaway. It particularly emphasizes the inhibition mechanisms of these decomposition products on the deflagration of CH_4, H_2,[28,29] and C_2H_4.[30,31]

Chain Reaction Mechanisms of CH_4 and H_2 Combustion. The deflagration of CH_4 and H_2 is primarily driven by continuous chain reactions, which often lead to severe hazards.

https://doi.org/10.1021/acssuschemeng.5c00573
ACS Sustainable Chem. Eng. XXXX, XXX, XXX−XXX

The currently recognized kinetic mechanisms for CH_4/H_2/air mixtures include GRI-Mech 3.0, USC-Mech II, Aramco mech 1.3, and San Diego mech mechanisms.[28,32]

Research has been conducted on the deflagration mechanism of CH_4/H_2/air mixtures, suggesting that the flame characteristics of CH_4/H_2/air mixtures can be integrated into a 21-step reduced mechanism.[29] Moreover, the fundamental reactions promoting free radical generation are R38, R155, and R156.[32] Among them, the laminar burning velocity of the CH_4/H_2 mixture is significantly influenced by the O and OH radicals produced in reaction R38.[28] It has also been suggested that R38 serves as the dominant chain-branching reaction in CH_4 deflagration, significantly promoting the chain reaction process. R31 is a significant chain-branching reaction and the most crucial exothermic reaction in hydrocarbon fuel combustion, serving as the primary source of H radicals in the reaction.[33] Additionally, it has been determined that the main reaction pathways of the CH_4/H_2 mixture involve CH_4, CH_3, CH_3O, CH_2O, HCO, CO, and CO_2.[28] Combined with previous research, the chain reactions that promote the deflagration of CH_4/H_2 and the main reaction pathways are summarized, as shown in Table 2.

Chain Reaction Mechanisms of C_2H_4 Combustion. Some studies have been conducted on the chain reactions during the deflagration of C_2H_4. It found that reactions R194, R96, R254, and R1 favor the consumption of C_2H_4. And the reaction R195 inhibits C_2H_4 consumption.[30] Other studies have found that 7 reactions were identified as the forward elementary reactions in C_2H_4 explosions, while 3 reactions were identified as the reverse elementary reactions.[31] Inhibiting the forward reactions or promoting the reverse reactions could significantly enhance the inhibition of C_2H_4 explosions. Furthermore, radicals such as CH_3, C_2H_3, H, O, HCO, CH_2CHO and OH play a critical role in the chain reaction process, and the consumption of these key radicals can terminate the chain propagation. Combined with previous research, the chain reactions that promote the deflagration of C_2H_4 are summarized, as shown in Table 3.

Fire Extinguishing Mechanisms of Fluorine-Containing Groups. Some studies have been conducted on the fire-extinguishing processes involving fluorine-containing groups. The reaction mechanisms of fluorine-containing groups such as CF_3, CF_2, CF, CF_2O and so on with free radicals and O_2 in the fire inhibition process were elucidated.[34] Furthermore, some other fire inhibition mechanisms of CF_3 and CF_2 also have been revealed, through the study of the extinguishing effects of CF_3I, CF_3Br and CF_3H on high-temperature methane flames.[35] Additionally, it has been concluded that CF, CF_2, CHF_2 and CHF can react with radicals in the combustion reaction through the research on the intermediate products of the extinguishing of CH_4-O_2 premixed flames by perfluoropropane.[36] By integrating previous research, the reaction mechanisms of fluorine-containing groups such as CF, CF_2, CF_3, etc. with radicals have been obtained, as shown in Table 4.

Additionally, Table 4 was integrated into a mechanism diagram of the reaction between fluorine-containing groups of HFE-7100 pyrolysis and free radicals, oxygen, and other substances, and the detailed reaction pathways were obtained, as shown in Figure 11.

The key chain reactions that occur during the deflagration of CH_4, H_2, and C_2H_4 have been summarized. The fire inhibition mechanisms of fluorine-containing groups have also been reviewed. The inhibition mechanism of HFE-7100 pyrolysis gas products on LIB thermal runaway gases deflagration is preliminarily analyzed in Figure 12, by integrating the reaction steps of fluorine-containing groups and active centers in the deflagration chain reaction depicted in Figure 11. Through analysis, it can be confirmed that during the fire inhibition process, the thermal decomposition of HFE-7100 produces fluorine-containing free radicals such as CF_3, CF_2, CF, and CHF_2. These radicals can react with the free radicals such as H, O, OH and so on present in the combustion chain reactions, thereby reducing the concentration of these radicals and interrupting the chain reactions, effectively contributing to the chemical inhibition of the deflagration.

CONCLUSIONS

This study experimentally examines the inhibitory effects of HFE-7100 on the deflagration of LIB thermal runaway gases and explores the underlying mechanisms, given the frequent occurrence of thermal runaway and deflagration incidents in LIBs. The peak temperature, peak pressure, and temperature ratio profiles are obtained by an Accelerating Rate Calorimeter (ARC). Additionally, pyrolysis experiments of HFE-7100 were conducted. Based on the experimental analysis and mechanistic discussion, the following conclusions are drawn:

(1) With the addition of HFE-7100, the peak temperature rise ratio during the thermal runaway of LIBs decreases. The rate of decrease in the peak temperature rise ratio is approximately positively correlated with battery capacity.

(2) HFE-7100 begins to decompose at 400 °C and is nearly completely decomposed by 850 °C. The gaseous products generated during the pyrolysis process mainly include $CF_3CF_2CF_2CHF_2$, $CF_3CF_2CF=CF_2$, $CF_3CF=CF_2$, and CHF_3.

(3) The fluorine-containing groups generated by the pyrolysis of HFE-7100 can react with the active centers in the combustion chain reaction, such as free radicals H, O, and OH, during the inhibition of LIB deflagration. This reaction reduces the concentration of these free radicals in the combustion chain reaction, thereby inhibiting the chain reaction and effectively inhibiting deflagration.

AUTHOR INFORMATION

Corresponding Author

Biao Zhou − *School of Emergency Management and Safety Engineering, China University of Mining and Technology (Beijing), Beijing 100083, China*; Email: zhoubiao1088@cumtb.edu.cn

Authors

Muying Ge − *School of Emergency Management and Safety Engineering, China University of Mining and Technology (Beijing), Beijing 100083, China*; orcid.org/0009-0004-0964-3659

Kai Wang − *School of Emergency Management and Safety Engineering, China University of Mining and Technology (Beijing), Beijing 100083, China*

Hideki Yoshioka − *Department of Architecture, Faculty of Engineering, The University of Tokyo, Tokyo 113-8654, Japan*

Jun Han − *College of Resources and Environment Engineering, Wuhan University of Science and Technology, Wuhan 430081, China*

https://doi.org/10.1021/acssuschemeng.5c00573
ACS Sustainable Chem. Eng. XXXX, XXX, XXX−XXX

Linbo Qin − *College of Resources and Environment Engineering, Wuhan University of Science and Technology, Wuhan 430081, China*
Zhenxiang Tao − *School of Emergency Management and Safety Engineering, China University of Mining and Technology (Beijing), Beijing 100083, China*
Wei Wang − *Shanghai Fire Science Technology Research Institute of MEM, Shanghai 200032, China*
Tao Chen − *Tianjin Fire Science Technology Research Institute of MEM, Tianjin 300381, China*

Complete contact information is available at: https://pubs.acs.org/10.1021/acssuschemeng.5c00573

Notes

The authors declare no competing financial interest.

■ ACKNOWLEDGMENTS

This work was supported by the Beijing Nova Program (No. Z211100002121102n), the Tianjin Science and Technology Plan Project (No. 22JCZDJC00880, No. 22JCZDJC00900), the Ordos key research and development program (No. YF20240026), Key Laboratory of Fire Protection Technology for Industry and Public Building Ministry of Emergency Management (No. 2023KLIB02), and State Key Laboratory Cultivation Base for Gas Geology and Gas Control (Henan Polytechnic University) (No. WS2021A01).

■ REFERENCES

(1) Zhong, G.; Mao, B.; Wang, C.; Jiang, L.; Xu, K.; Sun, J.; Wang, Q. Thermal runaway and fire behavior investigation of lithium ion batteries using modified cone calorimeter. *J. Therm. Anal. Calorim.* **2019**, *135* (5), 2879−2889.
(2) Roe, C.; Feng, X.; White, G.; Li, R.; Wang, H.; Rui, X.; Li, C.; Zhang, F.; Null, V.; Parkes, M.; Patel, Y.; Wang, Y.; Wang, H.; Ouyang, M.; Offer, G.; Wu, B. Immersion cooling for lithium-ion batteries − A review. *J. Power Sources* **2022**, *525*, No. 231094.
(3) Manetti, L. L.; Ribatski, G.; de Souza, R. R.; Cardoso, E. M. Pool boiling heat transfer of HFE-7100 on metal foams. *Exp. Therm. Fluid Sci.* **2020**, *113*, No. 110025.
(4) Rausch, M. H.; Kretschmer, L.; Will, S.; Leipertz, A.; Fröba, A. P. Density, Surface Tension, and Kinematic Viscosity of Hydrofluoroethers HFE-7000, HFE-7100, HFE-7200, HFE-7300, and HFE-7500. *J. Chem. Eng. Data* **2015**, *60* (12), 3759−3765.
(5) Liang, G.; Mudawar, I. Review of pool boiling enhancement by surface modification. *Int. J. Heat Mass Transfer* **2019**, *128*, 892−933.
(6) Teodori, E.; Teodori, E.; Moita, A. S. O. H. Empirical and Modeling-based correlations for pool boiling on microstructured surfaces. *Interfacial Phenom. Heat Transfer* **2014**, *2* (3), 273.
(7) Li, X.; Zhou, Z.; Zhang, M.; Zhang, F.; Zhou, X. A liquid cooling technology based on fluorocarbons for lithium-ion battery thermal safety. *J. Loss Prev. Process Ind.* **2022**, *78*, No. 104818.
(8) Tousi, M.; Najafi, M. Innovative hybrid nano/dielectric fluid cooling system for the new cylindrical shaped Li-ion batteries. *Int. J. Therm. Sci.* **2024**, *195*, No. 108634.
(9) El-Genk, M. S. Immersion cooling nucleate boiling of high power computer chips. *Energy Convers. Manage.* **2012**, *53* (1), 205−218.
(10) Febriyanto, R.; Pranoto, I.; Ariyadi, H. Thermal performance of serpentine channel immersion cooling for lithium-ion battery 18650 with HFE-7100. In *IOP Conference Series: Earth and Environmental Science*; IOP Publishing, 2023; Vol. *1281* DOI: 10.1088/1755-1315/1281/1/012066.
(11) Sadeh, M.; Tousi, M.; Sarchami, A.; Sanaie, R.; Kiani, M.; Ashjaee, M.; Houshfar, E. A novel hybrid liquid-cooled battery thermal management system for electric vehicles in highway fuel-economy condition. *J. Energy Storage* **2024**, *86*, No. 111195.
(12) Bai, P.; Xu, R.; Liu, M.; Jia, Z.; Sun, Z.; Wang, J.; Zhang, J.; Pei, J.; Zhang, Q.; Wang, J.; Cao, C.; Cao, X.; Yang, Y.; Zhang, J. Thermal Runaway Characteristics of LFP Batteries by Immersion Cooling. *ACS Appl. Energy Mater.* **2023**, *6* (13), 7205−7211.
(13) Zhou, H.; Dai, C.; Liu, Y.; Fu, X.; Du, Y. Experimental investigation of battery thermal management and safety with heat pipe and immersion phase change liquid. *J. Power Sources* **2020**, *473*, No. 228545.
(14) Meng, X.; Yang, K.; Zhang, M.; Gao, F.; Liu, Y.; Duan, Q.; Wang, Q. Experimental study on combustion behavior and fire extinguishing of lithium iron phosphate battery. *J. Energy Storage* **2020**, *30*, No. 101532.
(15) Koch, S.; Fill, A.; Birke, K. P. Comprehensive gas analysis on large scale automotive lithium-ion cells in thermal runaway. *J. Power Sources* **2018**, *398*, 106−112.
(16) Li, Y.; Bai, M.; Zhou, Z.; Lv, J.; Hu, C.; Gao, L.; Peng, C.; Li, Y.; Li, Y.; Song, Y. Experimental study of liquid immersion cooling for different cylindrical lithium-ion batteries under rapid charging conditions. *Therm. Sci. Eng. Prog.* **2023**, *37*, No. 101569.
(17) Li, Y.; Zhou, Z.; Hu, L.; Bai, M.; Gao, L.; Li, Y.; Liu, X.; Li, Y.; Song, Y. Experimental studies of liquid immersion cooling for 18650 lithium-ion battery under different discharging conditions. *Case Stud. Therm. Eng.* **2022**, *34*, No. 102034.
(18) Liu, J.; Zhang, Y.; Zhou, L.; Han, C.; He, T.; Wang, Z. Influencing factors of lithium-ion battery thermal runaway in confined space. *J. Energy Storage* **2023**, *73*, No. 109125.
(19) Zhang, H.; Meng, X.; Yang, Q.; Zhou, X. Toward Better Halon Substitutes: Theoretical and Experimental Studies on the Pyrolysis Mechanism and Fire-Suppressing Performance of C5F10O (Perfluoro-3-methyl-2-butanone). *ACS Sustainable Chem. Eng.* **2021**, *9* (3), 1272−1285.
(20) Singh, H. J.; Gour, N. K.; Srivastava, P. Computational studies on the thermal decomposition of the CH2FOCHFO radical. *Mol. Phys.* **2013**, *111* (24), 3756−3761.
(21) Yang, Q.; Gao, Y.; Yang, Y.; Zhou, X.; Zhang, H. Toward better halon substitutes: Effects of carbon chain length on pyrolytic and fire-suppressing mechanisms of perfluoroalkanes. *J. Mol. Struct.* **2024**, *1312*, No. 138589.
(22) Liu, F.; Hu, Q.; Jiang, C.; Xu, Y.; Yan, P.; Sui, X. The suppression performance of fluorinated cooling agents on the Lithium-ion Batteries fire based on the Accelerating Rate Calorimeter (ARC). *Therm. Sci. Eng. Progr.* **2023**, *42*, No. 101877.
(23) Sheng, M.; Valco, D.; Tucker, C. Heat Loss in Accelerating Rate Calorimetry Analysis and Thermal Lag for High Self-Heat Rates. *Org. Process Res. Dev.* **2021**, *25* (1), 108−119.
(24) Wang, K.; Wang, D.; Zhou, B.; Li, X. Fire extinguishing performance and fire extinguishing mechanism of perfluorobutyl methyl ether. *China Saf. Sci. J.* **2023**, *33* (12), 47−52.
(25) Zou, K.; Lu, S.; Chen, X.; Gao, E.; Cao, Y.; Bi, Y. Thermal and gas characteristics of large-format LiNi0.8Co0.1Mn0.1O2 pouch power cell during thermal runaway. *J. Energy Storage* **2021**, *39*, No. 102609.
(26) Mishra, D.; Shah, K.; Jain, A. Investigation of the Impact of Flow of Vented Gas on Propagation of Thermal Runaway in a Li-Ion Battery Pack. *J. Electrochem. Soc.* **2021**, *168* (6), No. 060555.
(27) Wang, H.; Xu, H.; Zhang, Z.; Wang, Q.; Jin, C.; Wu, C.; Xu, C.; Hao, J.; Sun, L.; Du, Z.; Li, Y.; Sun, J.; Feng, X. Fire and explosion characteristics of vent gas from lithium-ion batteries after thermal runaway: A comparative study. *eTransportation* **2022**, *13*, No. 100190.
(28) Li, R.; Luo, Z.; Wang, T.; Cheng, F.; Lin, H.; Zhu, X. Effect of initial temperature and H2 addition on explosion characteristics of H2-poor/CH4/air mixtures. *Energy* **2020**, *213*, No. 118979.
(29) Shi, L.; Meng, X.; Wu, Y. Numerical study on the propagation of CH4/H2 flame in a pipeline under different H2 enrichment conditions. *J. Cleaner Prod.* **2023**, *423*, No. 138689.
(30) Hu, S.; Li, R.; Nie, B.; Hong, Z.; Gao, J.; Yang, X.; Sun, X. Mechanism of Magnetic Field on the Explosive Radical of Ethylene Premixed Gas. *Hanneng Cailiao/Chin. J. Energ. Mater.* **2022**, *30* (12), 1252−1258.

(31) Wang, Y.; Yang, S.; Zhang, G.; Xu, Z.; Mao, W.; Ji, W. Explosion suppression characteristics and mechanism of ethylene by modified zeolite. *CIESC J.* **2023**, *74* (12), 5048.
(32) Hao, Q.; Luo, Z.; Wang, T.; Xie, C.; Zhang, S.; Bi, M.; Deng, J. The flammability limits and explosion behaviours of hydrogen-enriched methane-air mixtures. *Exp. Therm. Fluid Sci.* **2021**, *126*, No. 110395.
(33) Luo, Z.; Liang, H.; Wang, T.; Cheng, F.; Su, B.; Liu, L.; Liu, B. Evaluating the effect of multiple flammable gases on the flammability limit of CH4: Experimental study and theoretical calculation. *Process Saf. Environ. Prot.* **2021**, *146*, 369−376.
(34) Fallon, G. S.; Chelliah, H. K.; Linteris, G. T. Chemical effects of CF3H in extinguishing counterflow CO/air/H2 diffusion flames. *Symp. (Int.) Combust.* **1996**, *26* (1), 1395−1403.
(35) Babushok, V. I.; Linteris, G. T.; Meier, O. C. Combustion properties of halogenated fire suppressants. *Combust. Flame* **2012**, *159* (12), 3569−3575.
(36) Williams, B. A.; L' espÉrance, D. M.; Fleming, J. W. Intermediate species profiles in low-pressure methane/oxygen flames inhibited by 2-H heptafluoropropane: comparison of experimental data with kinetic modeling. *Combust. Flame* **2000**, *120* (1), 160−172.

https://doi.org/10.1021/acssuschemeng.5c00573
ACS Sustainable Chem. Eng. XXXX, XXX, XXX−XXX